# Supporting information for:

# Do Molecular Dynamics Force Fields Capture Conformational Dynamics of Alanine in Water?

Shuting Zhang,[†] Reinhard Schweitzer-Stenner,[‡] and Brigita Urbanc[*,†]

†*Department of Physics, Drexel University, Philadelphia, PA 19104, USA*

‡*Department of Chemistry, Drexel University, Philadelphia, PA 19104, USA*

¶*Faculty of Mathematics and Physics, University of Ljubljana, Slovenia*

E-mail: bu25@drexel.edu

Fax: (215) 895-5934

# Supporting Information Tables

Table S1: **Statistical uncertainties of Karplus parameters for J coupling constants.**[S1]

| J-coupling [Hz] | A | B | C |
|---|---|---|---|
| $3J(H^N H^{C_\alpha})$ | 0.11 | 0.04 | 0.09 |
| $3J(H^{C_\alpha} C)$ | 0.07 | 0.08 | 0.04 |
| $3J(H^N C_\beta)$ | 0.07 | 0.04 | 0.03 |
| $3J(H^N C)$ | 0.14 | 0.06 | 0.02 |

Table S2: **J coupling constants for GAG calculated for different force fields and Gaussian model alongside the experimental values and the corresponding uncertainties used in $\chi^2_J$ calculations.** The uncertainties are calculated by combining Eqs. (2) and (4).

| | $^3J(H^N H^{C_\alpha})$ | $^3J(H^N C')$ | $^3J(H^{C_\alpha} C')$ | $^3J(H^N C_\beta)$ | $^1J(N C_\alpha)$ |
|---|---|---|---|---|---|
| Gaussian | 6.00 | 1.09 | 1.89 | 1.95 | 11.39 |
| Amber ff14SB | 6.25 | 1.10 | 1.69 | 1.80 | 11.27 |
| Amber ff99SBnmr1 | 6.70 | 0.95 | 1.85 | 1.69 | 11.14 |
| Amber ff03ws | 6.64 | 1.22 | 1.80 | 1.56 | 11.21 |
| OPLS-AA/L | 7.37 | 0.85 | 2.01 | 1.47 | 10.87 |
| OPLS-AA/M | 7.19 | 0.81 | 1.94 | 1.61 | 11.28 |
| Charmm36 | 6.37 | 1.24 | 2.05 | 1.67 | 11.21 |
| Experimental | 6.11 | 1.19 | 1.9 | 2.09 | 11.28 |
| Uncertainty | 0.11 | 0.08 | 0.13 | 0.09 | 0.07 |

Table S3: **Populations of four mesostates of alanine in GAG in different force fields.**

| Force field | pPII | $\beta$t | a$\beta$ | right-handed $\alpha$-helix |
|---|---|---|---|---|
| Amber ff14SB | 0.55 | 0.07 | 0.13 | 0.09 |
| Amber ff99SBnmr1 | 0.44 | 0.14 | 0.08 | 0.12 |
| Amber ff03ws | 0.41 | 0.10 | 0.19 | 0.07 |
| OPLS-AA/L | 0.39 | 0.16 | 0.12 | 0.08 |
| OPLS-AA/M | 0.51 | 0.17 | 0.11 | 0.02 |
| CHARMM36 | 0.51 | 0.09 | 0.12 | 0.06 |
| Gaussian | 0.59 | 0.16 | 0.02 | 0.02 |

Table S4: **J coupling constants for AAA calculated for different force fields and Gaussian model alongside the experimental values and the corresponding uncertainties used in $\chi^2_J$ calculations.** The uncertainties are calculated by combining Eqs. (2) and (4).

| | $^3J(H^NH^{C_\alpha})$ | $^3J(H^NC')$ | $^3J(H^{C_\alpha}C')$ | $^3J(H^NC_\beta)$ | $^1J(NC_\alpha)$ | $^3J(CC')$ |
|---|---|---|---|---|---|---|
| Gaussian | 5.66 | 1.11 | 1.58 | 2.07 | 11.32 | 0.61 |
| Amber ff14SB | 6.07 | 1.13 | 1.70 | 1.87 | 11.41 | 0.79 |
| Amber ff99SBnmr1 | 6.45 | 1.00 | 1.78 | 1.80 | 11.44 | 0.79 |
| Amber ff03ws | 6.56 | 1.27 | 1.78 | 1.56 | 11.61 | 1.14 |
| OPLS-AA/L | 7.36 | 0.78 | 2.00 | 1.55 | 11.16 | 0.96 |
| OPLS-AA/M | 7.13 | 0.76 | 1.93 | 1.67 | 11.40 | 0.87 |
| Charmm36 | 6.12 | 1.26 | 2.00 | 1.76 | 11.34 | 0.85 |
| Experimental | 5.68 | 1.13 | 1.84 | 2.39 | 11.34 | 0.25 |
| Uncertainty | 0.11 | 0.08 | 0.13 | 0.09 | 0.07 | 0.10 |

Table S5: **Populations of four mesostates of alanine in AAA in different force fields.**

| Force field | pPII | $\beta$t | a$\beta$ | right-handed $\alpha$-helix |
|---|---|---|---|---|
| Amber ff14SB | 0.63 | 0.07 | 0.10 | 0.07 |
| Amber ff99SBnmr1 | 0.57 | 0.15 | 0.07 | 0.07 |
| Amber ff03ws | 0.47 | 0.12 | 0.22 | 0.04 |
| OPLS-AA/L | 0.40 | 0.17 | 0.11 | 0.10 |
| OPLS-AA/M | 0.55 | 0.18 | 0.10 | 0.02 |
| CHARMM36 | 0.57 | 0.09 | 0.11 | 0.04 |
| Gaussian | 0.76 | 0.09 | 0.03 | 0.03 |

Table S6: **Lifetimes of pPII for alanine in GAG and AAA in different force fields.**

| Peptide | Force field | $p_0$ | $\tau$ [ps] | $R^2$ |
|---|---|---|---|---|
| GAG | Amber ff14SB | 0.21 | 10.23 | 0.9943 |
| | Amber ff99SBnmr1 | 0.37 | 6.13 | 0.9964 |
| | Amber ff03ws | 0.37 | 5.90 | 0.9848 |
| | OPLS-AA/L | 0.54 | 4.44 | 0.9961 |
| | OPLS-AA/M | 0.50 | 4.77 | 0.9980 |
| | CHARMM36 | 0.29 | 7.68 | 0.9948 |
| AAA | Amber ff14SB | 0.16 | 13.08 | 0.9912 |
| | Amber ff99SBnmr1 | 0.36 | 5.72 | 0.9858 |
| | Amber ff03ws | 0.37 | 5.76 | 0.9906 |
| | OPLS-AA/L | 0.56 | 4.13 | 0.9931 |
| | OPLS-AA/M | 0.45 | 4.98 | 0.9936 |
| | CHARMM36 | 0.27 | 7.97 | 0.9905 |

Table S7: **Lifetimes of $\beta$t for alanine in GAG and AAA in different force fields.**

| peptide | Force field | $p_0$ | $\tau$ [ps] | $R^2$ |
|---|---|---|---|---|
| GAG | Amber ff14SB | 7.32 | 0.94 | 1.0000 |
| | Amber ff99SBnmr1 | 2.67 | 1.53 | 0.9996 |
| | Amber ff03ws | 4.15 | 1.22 | 0.9966 |
| | OPLS-AA/L | 3.17 | 1.33 | 0.9998 |
| | OPLS-AA/M | 3.30 | 1.37 | 1.0000 |
| | CHARMM36 | 4.81 | 1.14 | 1.0000 |
| AAA | Amber ff14SB | 7.04 | 0.96 | 1.0000 |
| | Amber ff99SBnmr1 | 2.45 | 1.59 | 0.9998 |
| | Amber ff03ws | 3.41 | 1.34 | 0.9999 |
| | OPLS-AA/L | 2.51 | 1.59 | 0.9999 |
| | OPLS-AA/M | 2.42 | 1.62 | 1.0000 |
| | CHARMM36 | 5.07 | 1.11 | 1.0000 |

Table S8: **Lifetimes of a$\beta$ for alanine in GAG and AAA in different force fields.**

| peptide | Force field | $p_0$ | $\tau$ [ps] | $R^2$ |
|---|---|---|---|---|
| GAG | Amber ff14SB | 0.63 | 4.01 | 0.9987 |
| | Amber ff99SBnmr | 1.59 | 2.07 | 0.9992 |
| | Amber ff03ws | 0.60 | 4.12 | 1.0000 |
| | OPLS-AA/L | 0.96 | 2.58 | 0.9980 |
| | OPLS-AA/M | 1.35 | 2.28 | 0.9983 |
| | CHARMM36 | 0.97 | 2.81 | 0.9966 |
| AAA | Amber ff14SB | 0.59 | 4.13 | 0.9942 |
| | Amber ff99SBnmr1 | 1.69 | 1.95 | 0.9978 |
| | Amber ff03ws | 0.55 | 4.27 | 0.9925 |
| | OPLS-AA/L | 0.99 | 2.75 | 0.9953 |
| | OPLS-AA/M | 1.31 | 2.27 | 0.9976 |
| | CHARMM36 | 1.02 | 2.70 | 0.9978 |

Table S9: **Lifetimes of right-handed $\alpha$-helix for alanine in GAG and AAA in different force fields.**

| peptide | Force field | $p_0$ | $\tau$ [ps] | $R^2$ |
|---|---|---|---|---|
| GAG | Amber ff14SB | 0.88 | 3.10 | 0.9992 |
| | Amber ff99SBnmr1 | 0.81 | 3.33 | 0.9980 |
| | Amber ff03ws | 0.71 | 3.57 | 0.9975 |
| | OPLS-AA/L | 0.78 | 3.40 | 0.9984 |
| | OPLS-AA/M | 1.05 | 2.79 | 0.9965 |
| | CHARMM36 | 0.72 | 3.51 | 0.9967 |
| AAA | Amber ff14SB | 0.47 | 4.85 | 0.9966 |
| | Amber ff99SBnmr1 | 0.45 | 5.10 | 0.9966 |
| | Amber ff03ws | 0.40 | 5.93 | 0.9917 |
| | OPLS-AA/L | 0.83 | 3.13 | 0.9924 |
| | OPLS-AA/M | 0.50 | 4.82 | 0.9903 |
| | CHARMM36 | 0.37 | 6.02 | 0.9903 |

# Supporting Information Figures

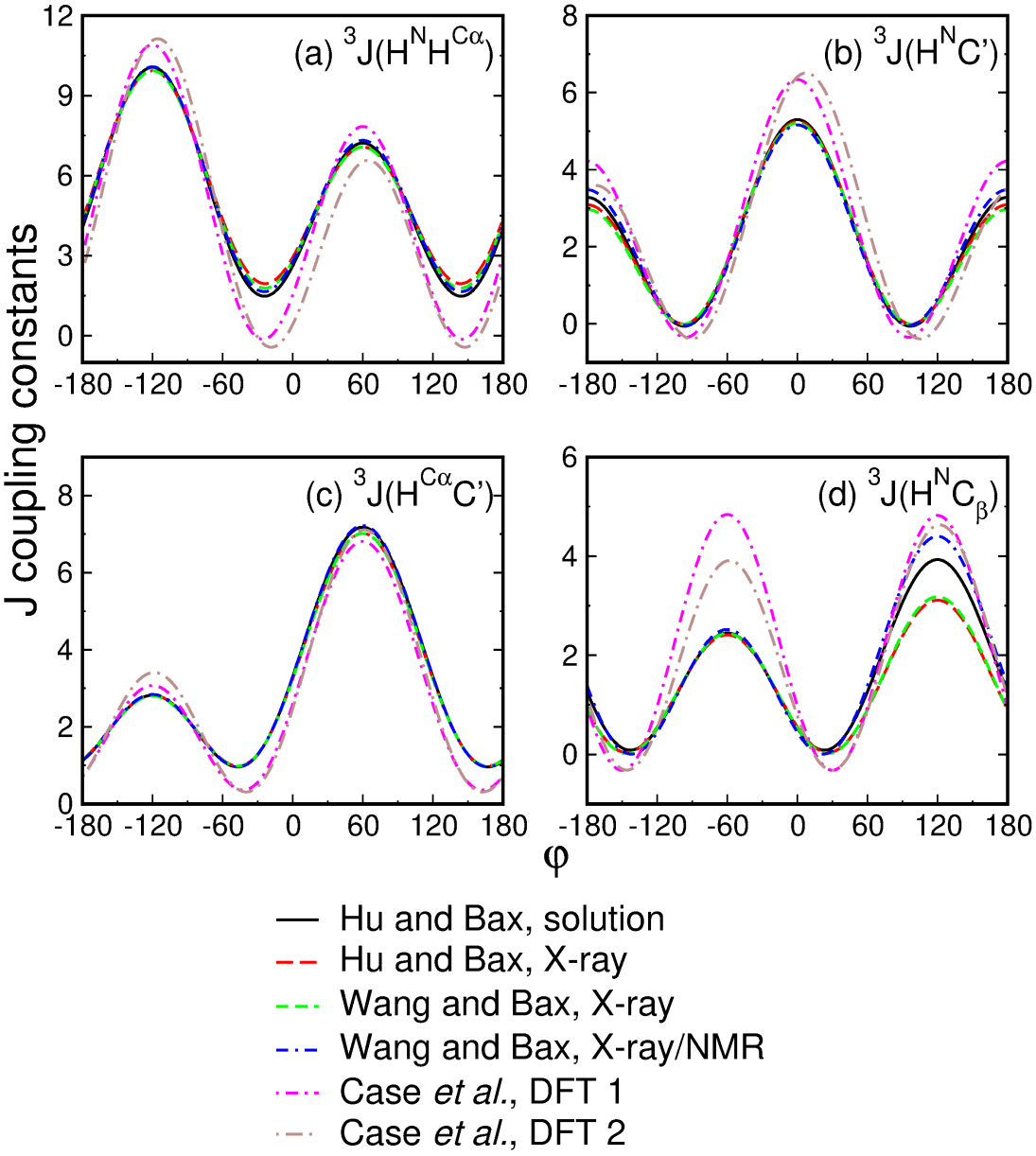


Figure S1: **Four J coupling constants as a function of $\phi$.** Different sets of Karplus parameters reported by Hu and Bax,[S2] Wang and Bax,[S1] and Case, Scheurer, and Brüschweiler[S3] are plotted for comparison.

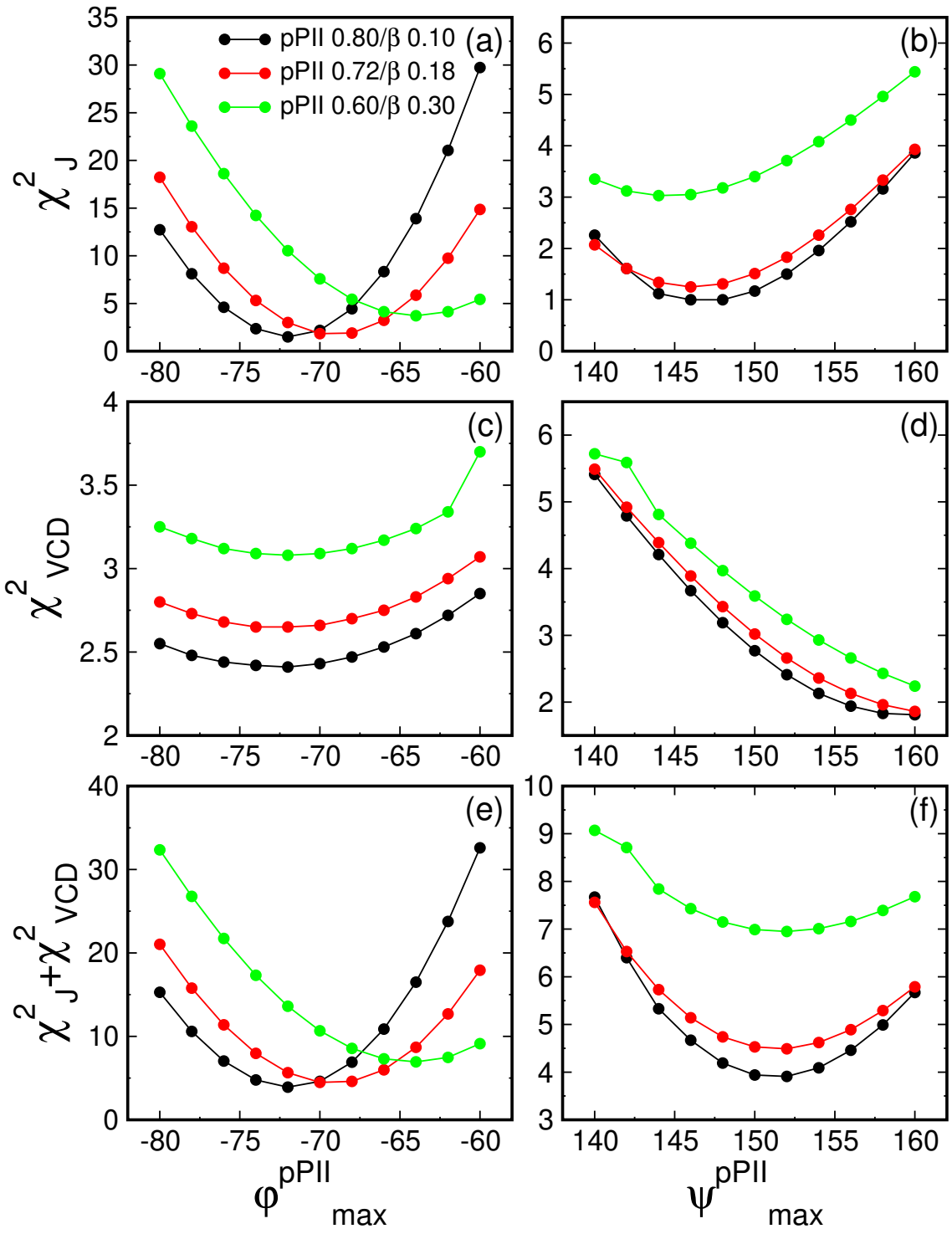


Figure S2: **Sensitivity analysis for pPII within the Gaussian model of alanine in GAG.** The weight of the Gaussian sub-distribution corresponding to the pPII state was varied and its center was shifted in (a,c,e) $\phi$ and (b,d,f) $\psi$ directions to show the resulting effects on (a,b) $\chi^2_J$, (c,d) $\chi^2_{VCD}$, and (e,f) their sum.

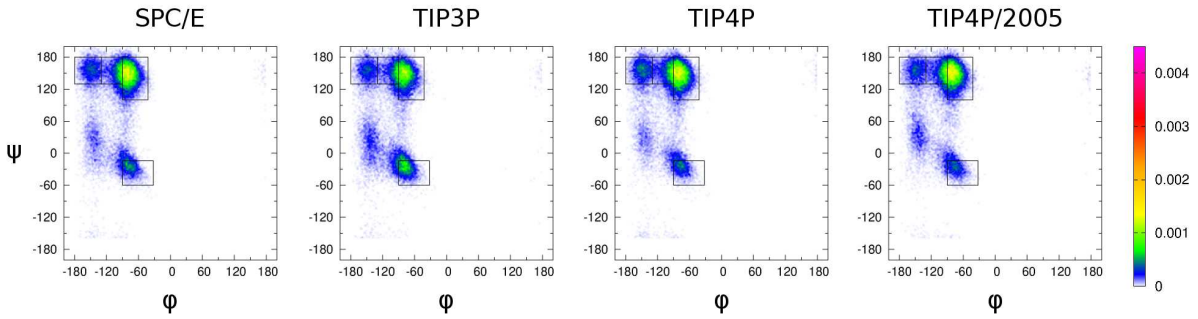


Figure S3: **Ramachandran distributions for alanine in GAG predicted by OPLS-AA/L.** Normalized distributions of backbone dihedral angles $\phi$ and $\psi$ are derived from MD simulations using OPLS-AA/L combined with four different water model. Black frames correspond to the four mesostates (a$\beta$, $\beta$t, pPII, and $\alpha$-helix) defined in *Methods*. The color of each $2^\circ \times 2^\circ$ bin corresponds to the occupation probability as marked on the color scale.

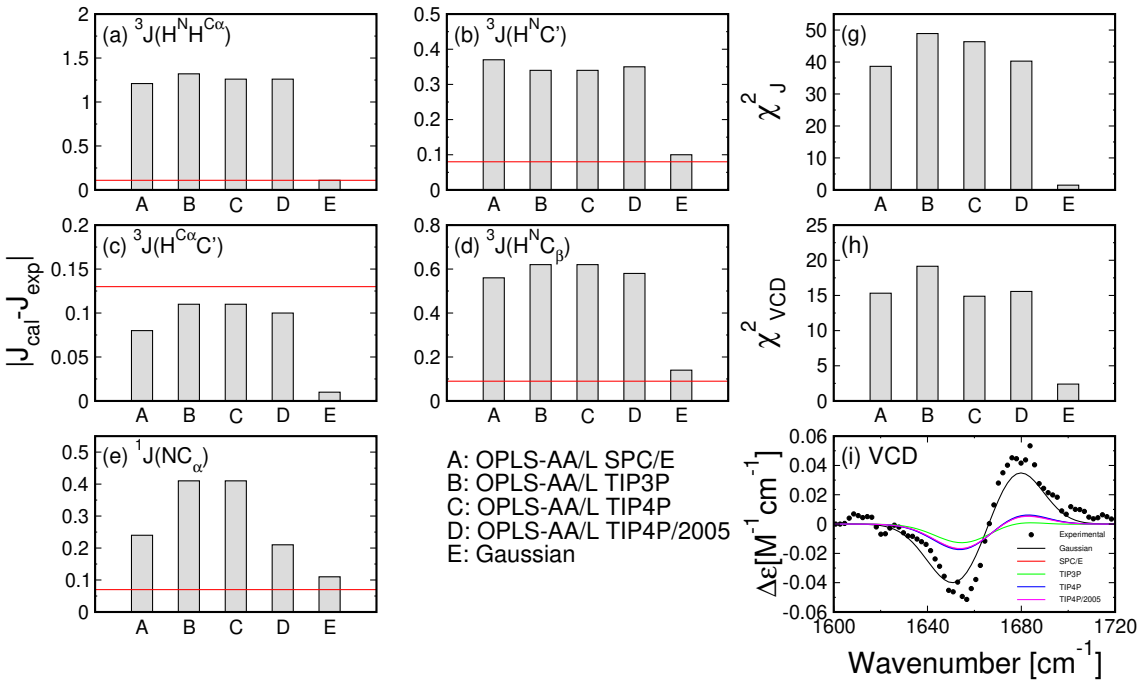


Figure S4: **Comparison between OPLS-AA/L and experimental J coupling constants and VCD amide I' profiles for alanine in GAG.** Five J-coupling constants and VCD amide I' profile are calculated from the Ramachandran distribution obtained for each water model combined with OPLS-AA/L as well as the Gaussian model to facilitated a direct comparison to experimental data. (a-e) Differences between the calculated and experimental values ($|J_{cal} - J_{exp}|$) are displayed for each of the five J-coupling constants. The red lines correspond to experimental errors. (g-h) The $\chi^2_J$ and $\chi^2_{VCD}$ values as defined in *Methods* measure overall deviations from experimental data. (i) The calculated VCD profiles predicted by the Gaussian model and different water models combined with OPLS-AA/L are compared to the experimental VCD profile.

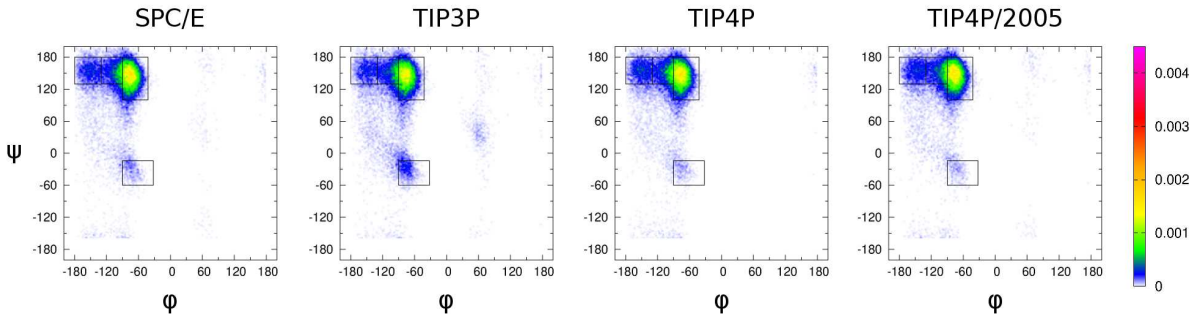


Figure S5: **Ramachandran plots for alanine in GAG as predicted by OPLS-AA/M.** Normalized distributions of backbone dihedral angles $\phi$ and $\psi$ are derived from MD simulations using OPLS-AA/M combined with four different water model. Black frames correspond to the four mesostates (a$\beta$, $\beta$t, pPII, and $\alpha$-helix) defined in *Methods*. The color of each $2^\circ \times 2^\circ$ bin corresponds to the occupation probability as marked on the color scale.

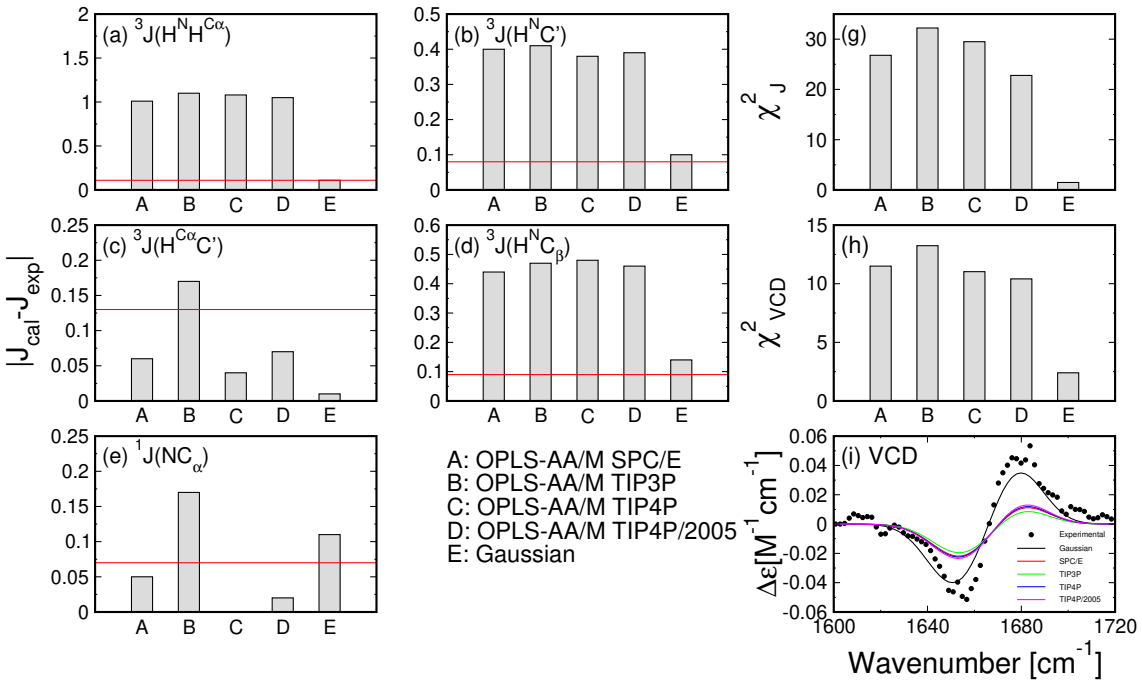


Figure S6: **Comparison between OPLS-AA/M and experimental J coupling constants and VCD amide I' profiles for alanine in GAG.** Five J-coupling constants and VCD amide I' profile are calculated from the Ramachandran distribution obtained for each water model combined with OPLS-AA/M as well as the Gaussian model to facilitated a direct comparison to experimental data. (a-e) Differences between the calculated and experimental values ($|J_{cal} - J_{exp}|$) are displayed for each of the five J-coupling constants. The red lines correspond to experimental errors. (g-h) The $\chi^2_J$ and $\chi^2_{VCD}$ values as defined in *Methods* measure overall deviations from experimental data. (i) The calculated VCD profiles predicted by the Gaussian model and different water models combined with OPLS-AA/M are compared to the experimental VCD profile.

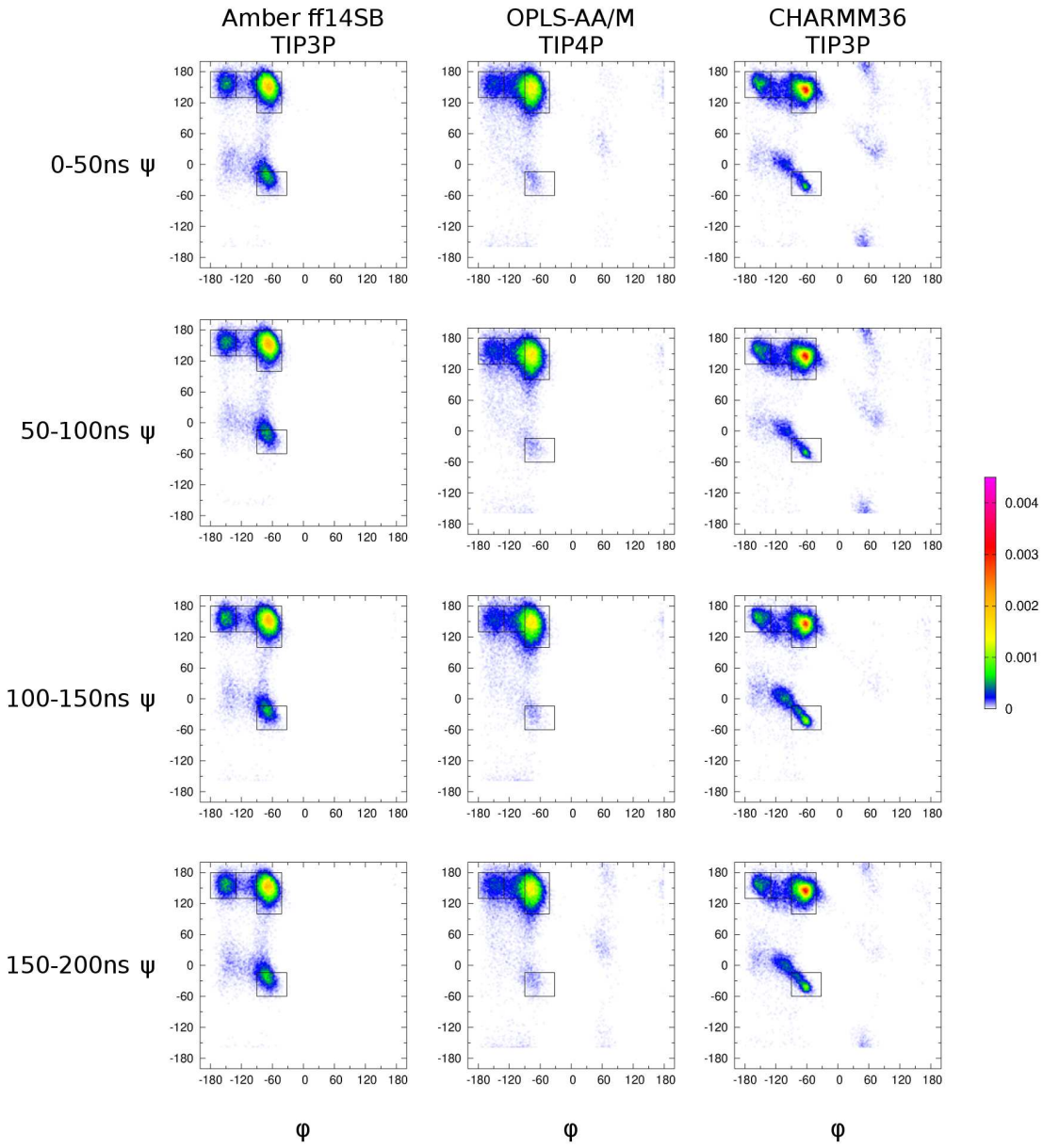


Figure S7: **Time evolution of Ramachandran plots for alanine in GAG in different force fields.** Ramachandran distributions are derived using the following time widows: 0-50 ns, 50-100 ns, 100-150 ns, and 150-200 ns. Black frames on Ramachandran plots correspond to the four mesostates defined in *Methods*.

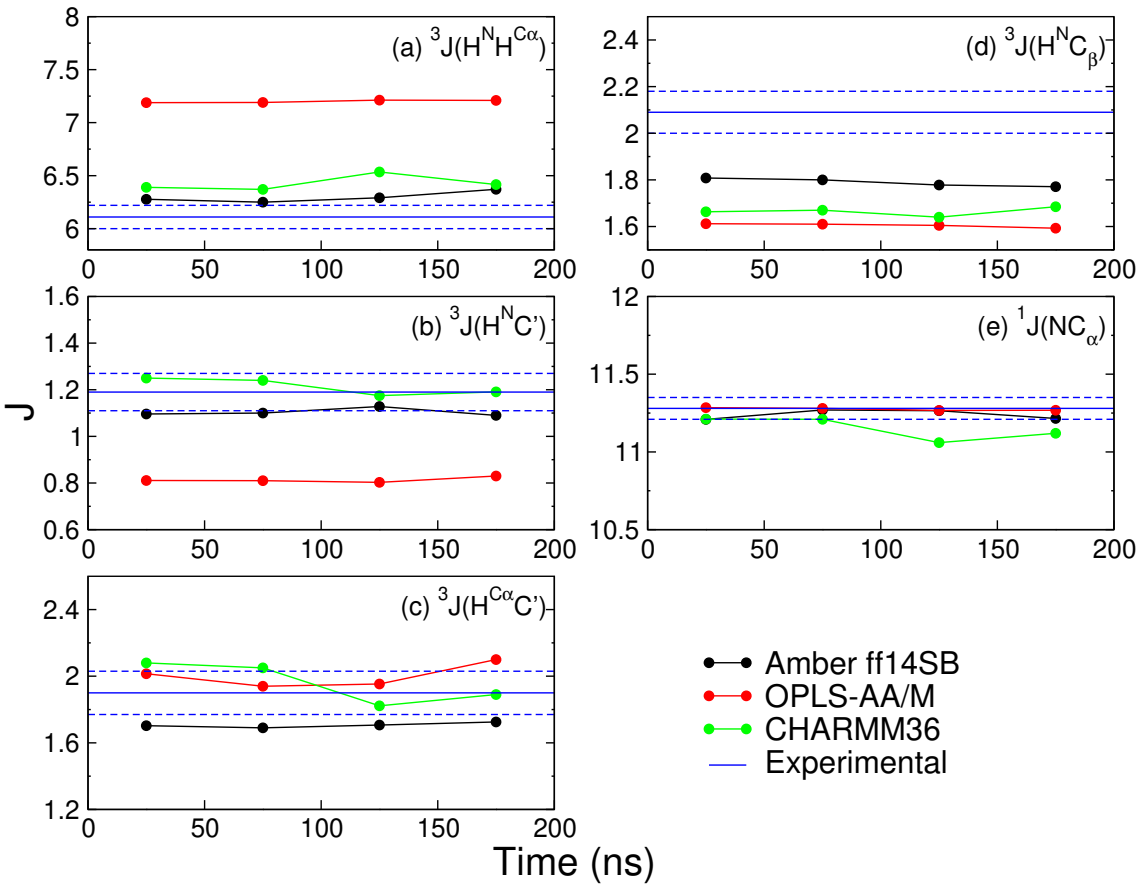


Figure S8: **Time evolution of J coupling constants for alanine in GAG in different force fields.** Each J coupling constant is calculated for a 50 ns time interval along the 200 ns–long trajectory. Solid blue lines are experimental values and dashed blue lines correspond to the uncertainties used in the $\chi^2_J$ calculations.

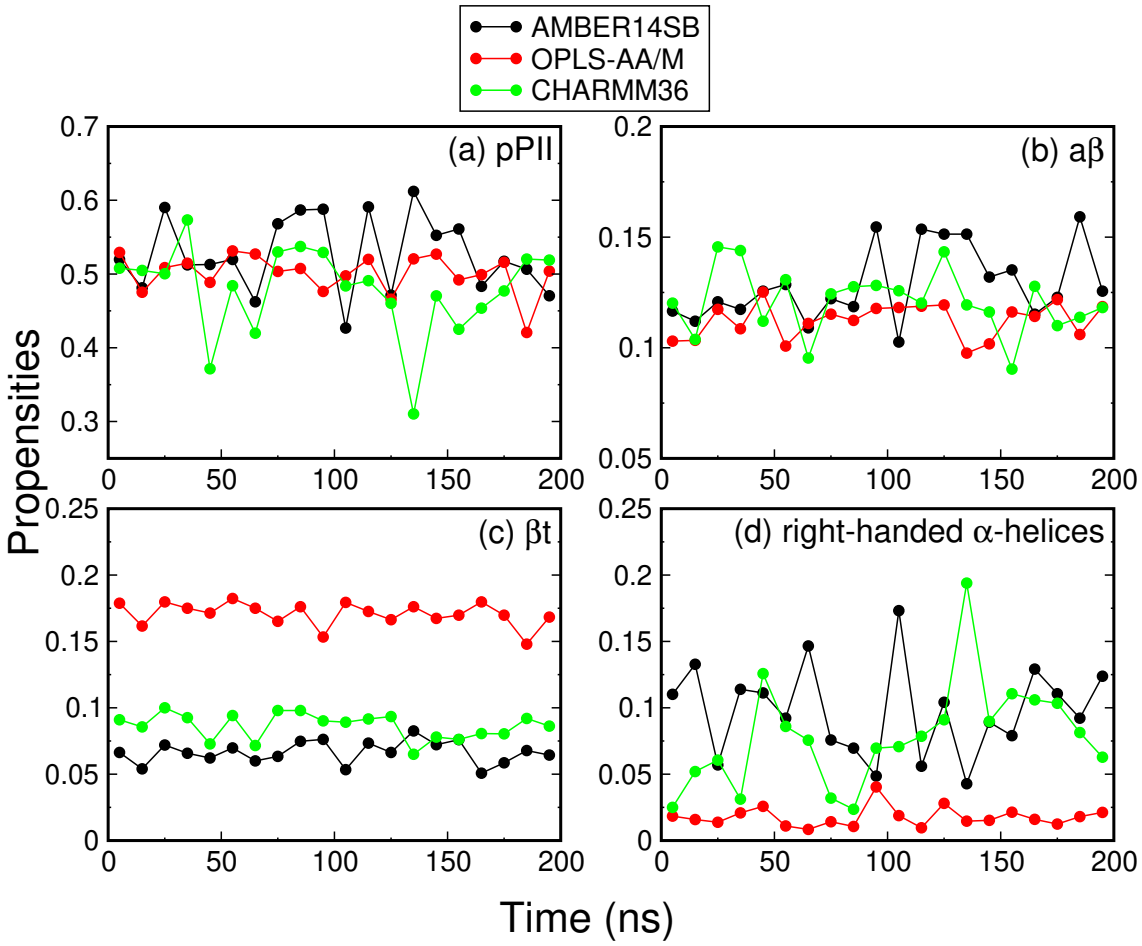


Figure S9: **Time evolution of mesostate populations for alanine in GAG in different force fields.** Each mesostate population is calculated as an average over 10 ns time interval.

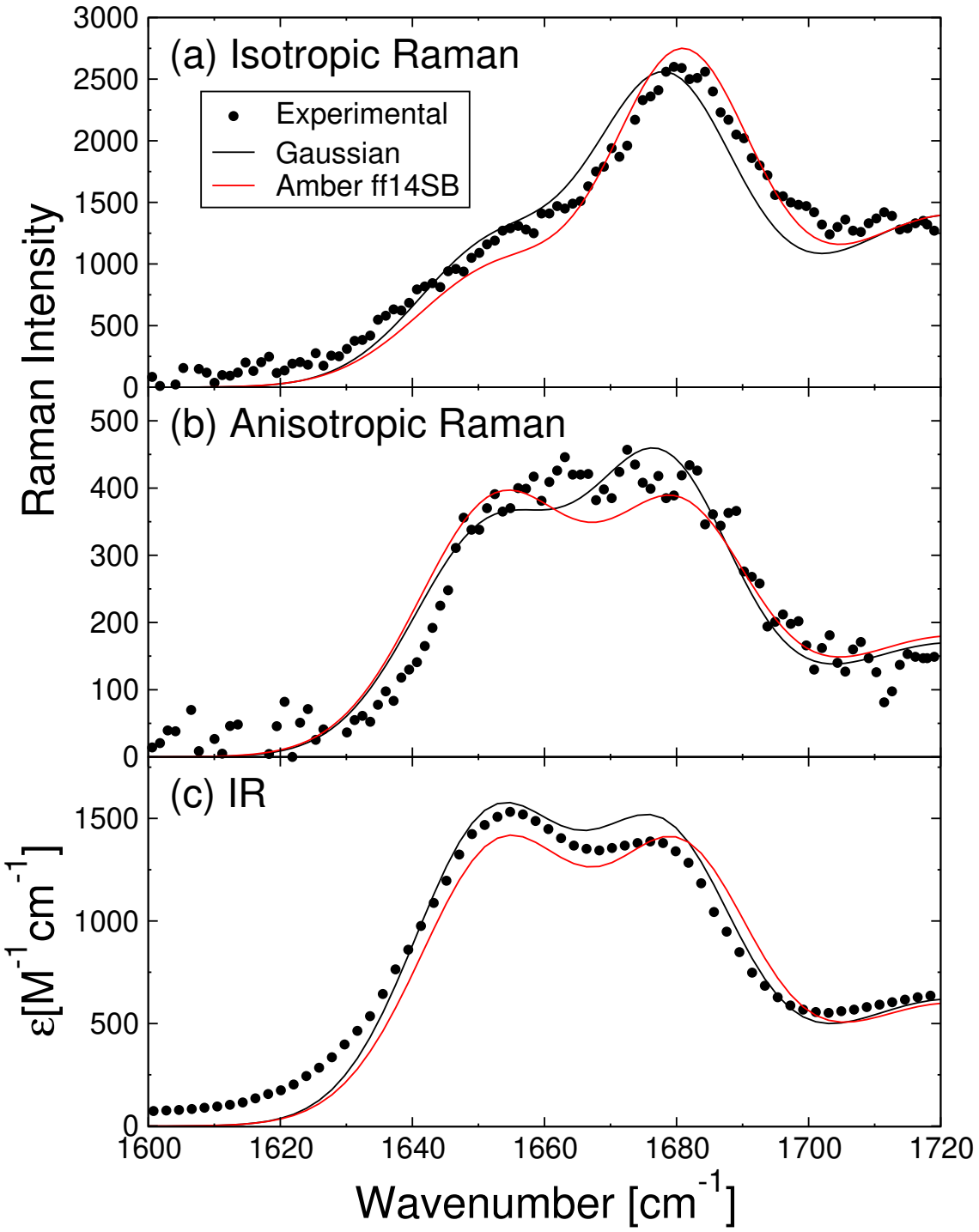


Figure S10: **Amide I' profiles for alanine in GAG.** Experimental amide I' profiles derived from (a) isotropic Raman, (b) anisotropic Raman, and (c) IR spectroscopy measurements are compared to predictions of the Gaussian model and Amber ff14SB combined with TIP3P.

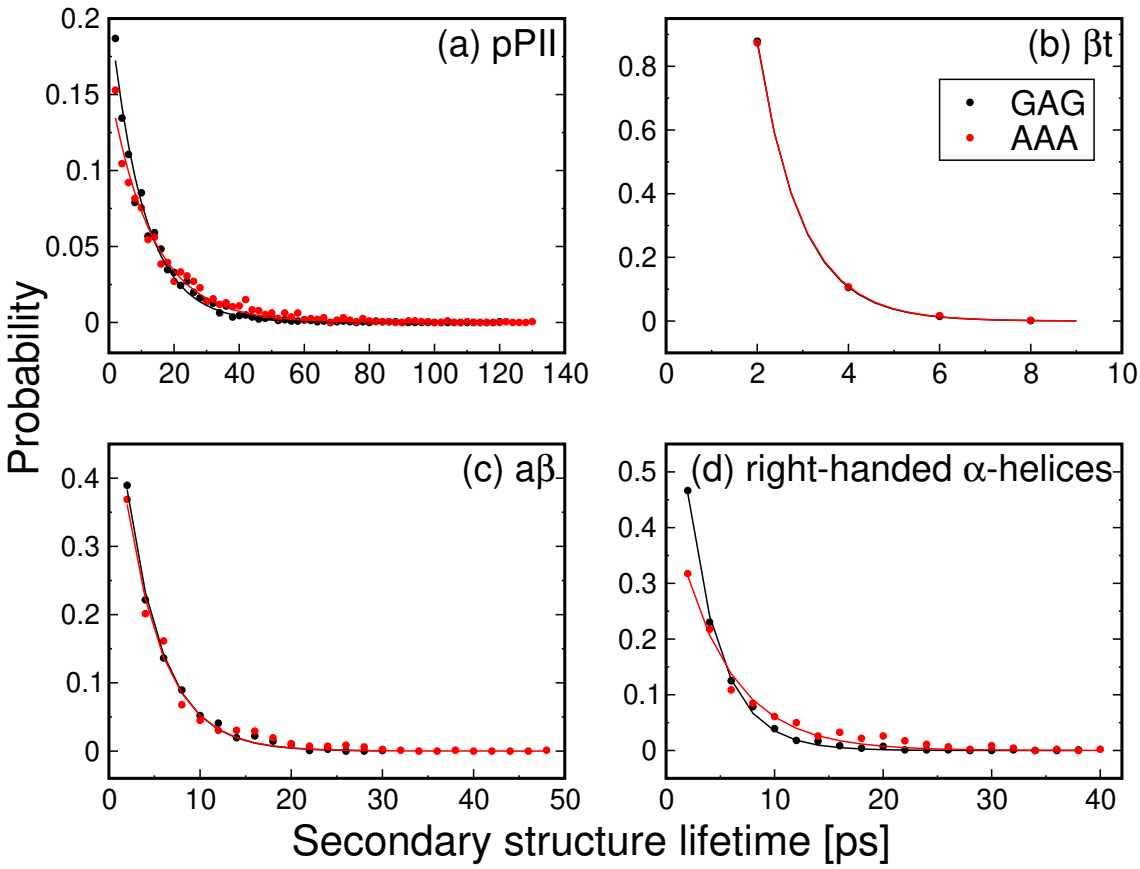


Figure S11: **Distribution of mesostate lifetimes of GAG and AAA in Amber ff14SB.** The mesostate lifetimes and the corresponding distributions were calculated and exponentially fitted (black and red curves for GAG and AAA, respectively) as described in *Methods*.

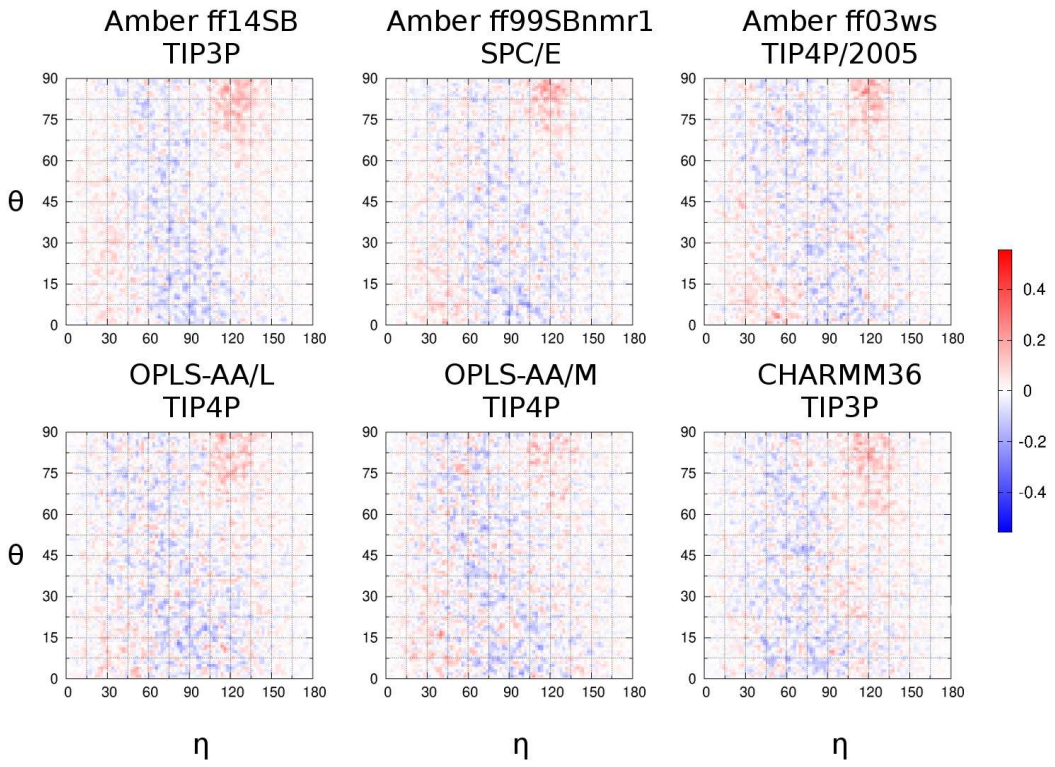


Figure S12: **AAA to GAG difference in the water orientation distribution around the side chain of alanine.** For each force field, the water orientation distribution obtained for the side chain of alanine in GAG is subtracted from the water orientation distribution obtained for the side chain of the central alanine in AAA and the difference is normalized to the maximum value across all water orientation distributions ($45 \times 10^{-5}$), such that the scale on the five difference plots corresponds to relative (fractional) changes. Positive values, marked in red, correspond to water orientations that are more abundant around the side chain of the central alanine in AAA. Negative values, marked in blue, correspond to water orientations that are more abundant around the side chain of alanine in GAG.

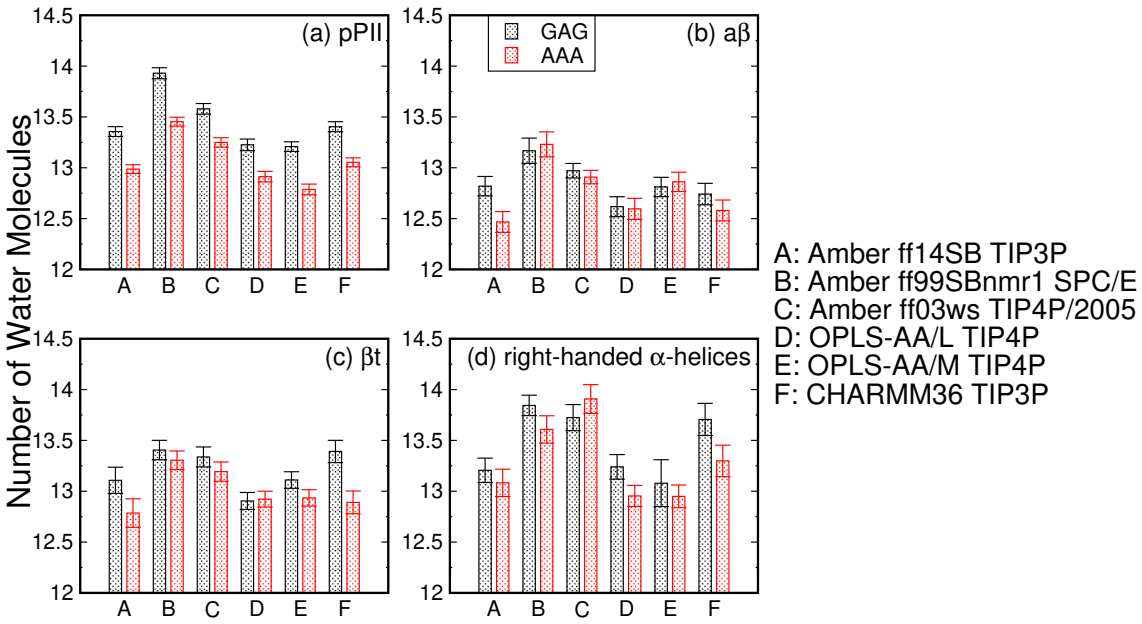


Figure S13: **Number of water molecules within the hydration layer around the side chain of alanine.** The average number of water molecules for each force field / water model for alanine conformations in (a) pPII, (b) a$\beta$, (c) $\beta$t, and (d) right handed $\alpha$-helix states. The error bars correspond to SEM values.

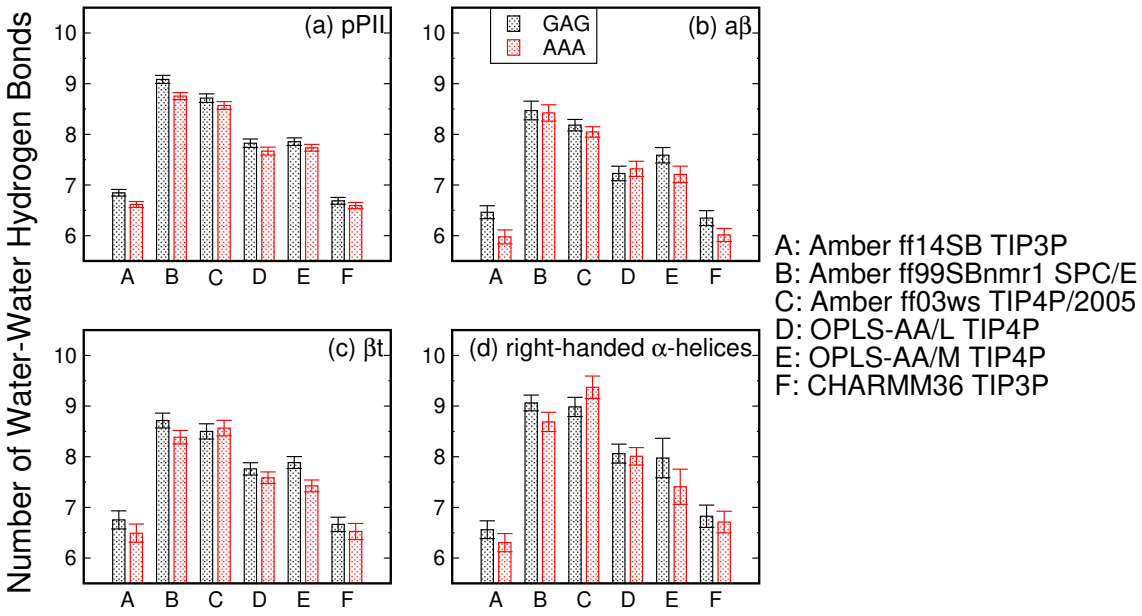


Figure S14: **Number of water-water hydrogen bonds within the hydration layer around the side chain of alanine.** The average number of water-water hydrogen bonds in the hydration layer around the central alanine is calculated for each force field / water model for alanine conformations in (a) pPII, (b) a$\beta$, (c) $\beta$t, and (d) right handed $\alpha$-helix states. The error bars correspond to SEM values.

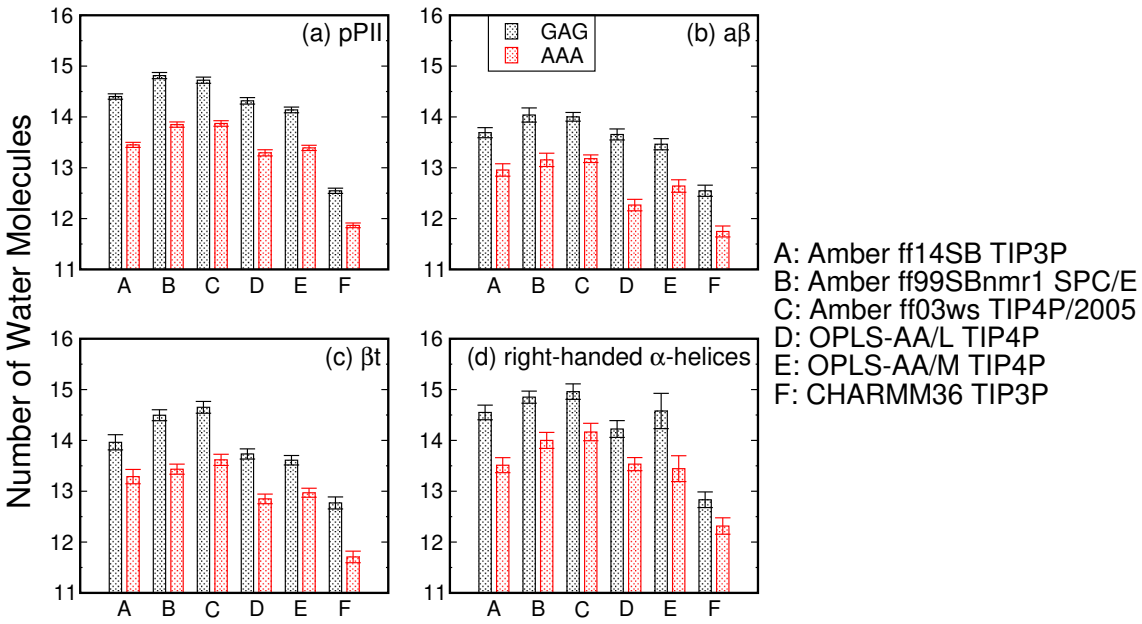


Figure S15: **Number of water molecules within the hydration layer around the backbone of alanine.** The average number of water molecules for each force field / water model for alanine conformations in (a) pPII, (b) a$\beta$, (c) $\beta$t, and (d) right handed $\alpha$-helix states. The error bars correspond to SEM values.

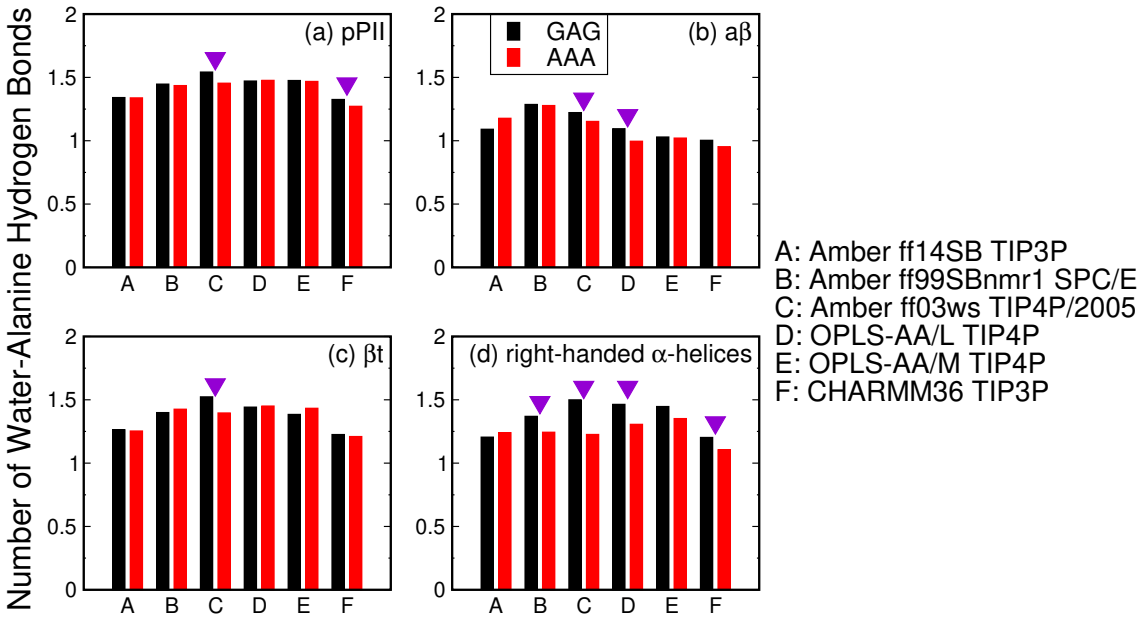


Figure S16: **Hydrogen bonding between water and alanine in GAG and AAA.** The average number of hydrogen bonds between water and central alanine is calculated for each force field / water model for alanine conformations in (a) pPII, (b) a$\beta$, (c) $\beta$t, and (d) right handed $\alpha$-helix states. The error bars correspond to SEM values. Purple triangles mark the data for which the GAG→AAA difference in the average numbers of hydrogen bonds is statistically significant.

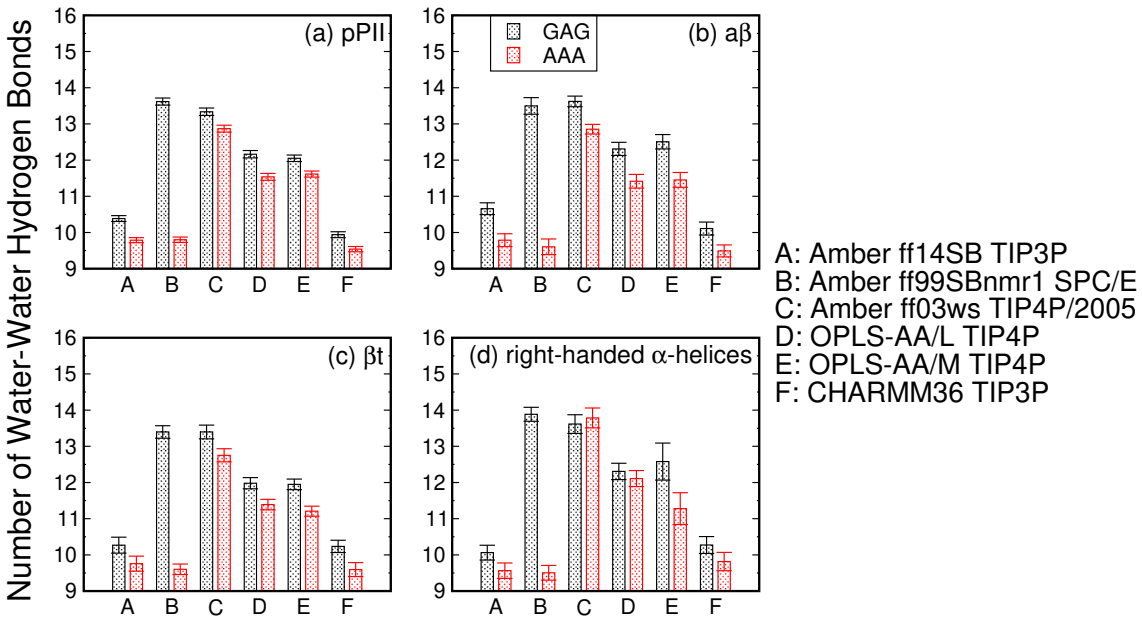


Figure S17: **Number of water-water hydrogen bonds within the hydration layer around the central alanine.** The average number of water-water hydrogen bonds in the hydration layer around the central alanine is calculated for each force field / water model for alanine conformations in (a) pPII, (b) a$\beta$, (c) $\beta$t, and (d) right handed $\alpha$-helix states. The error bars correspond to SEM values.

# References

(S1) Wang, A. C.; Bax, A. Determination of the backbone dihedral angles $\phi$ in human ubiquitin from reparametrized empirical Karplus equations. *J. Am. Chem. Soc.* **1996**, *118*, 2483–2494.

(S2) Hu, J.-S.; Bax, A. Determination of $\phi$ and $\chi_1$ angles in proteins from $^{13}$C–$^{13}$C three-bond J couplings measured by three-dimensional heteronuclear NMR. How planar is the peptide bond? *J. Am. Chem. Soc.* **1997**, *119*, 6360–6368.

(S3) Case, D. A.; Scheurer, C.; Brüschweiler, R. Static and dynamic effects on vicinal scalar J couplings in proteins and peptides: A MD/DFT analysis. *J. Am. Chem. Soc.* **2000**, *122*, 10390–10397.